

2D mappings of ICRF-induced SOL density modifications on JET

L. Colas¹, P. Jacquet², V. Bobkov³, M. Brix², L. Meneses⁴, K. Kirov², E. Lerche^{2,5}, C.C. Klepper⁶, M. Goniche¹, A. Křivská⁵, P. Dumortier^{2,5}, A. Czarnecka⁷ and JET contributors*

EUROfusion Consortium, JET, Culham Science Centre, Abingdon, OX14 3DB, UK

¹*CEA, IRFM, F-13108 Saint Paul Lez Durance, France.*

²*CCFE, Culham Science Centre, Abingdon, OX14 3DB, UK.*

³*Max-Planck-Institut für Plasmaphysik, Garching, Germany.*

⁴*Instituto de Plasmas e Fusão Nuclear, IST, Universidade de Lisboa, Lisboa, Portugal.*

⁵*LPP-ERM-KMS, TEC partner, Brussels, Belgium.*

⁶*Oak Ridge National Laboratory, PO Box 2008, Oak Ridge, USA.*

⁷*IPPLM, Hery 23 Str., 01-497 Warsaw, Poland.*

Waves in the Ion Cyclotron Range of Frequencies (ICRF, 20-80MHz) provide core ion heating in tokamaks and are used to limit impurity accumulation in high-performance JET scenarios [1][2]. Before reaching the core, these radiofrequency (RF) waves, excited at the Low-Field Side of the torus, interact with the Scrape-Off-Layer (SOL), causing enhanced wall sputtering, heat loads and local density (n_e) changes with a complex 3D geometry. Extending previous studies on JET [3-5], this paper aims at mapping RF-induced SOL n_e patterns in 2D. This puts constraints on SOL RF modelling and provides hints for locating RF-specific W-sources on the JET ITER-Like-Wall (ILW), similar to the ITER vessel.

I. Experimental setup and 2D mapping technique

At JET, ICRF waves were excited at a frequency of 42MHz by phased toroidal arrays of four poloidal RF current straps (A2 antennas [6]) as well as a 2×4 ITER-like array (ILA [7]). Four A2 antennas (named A-D) are located toroidally around the torus, while the ILA is placed between A and B (see figure 1). Upper and Lower halves of the ILA can be operated independently of D and of the pair A+B, whose feeding transmission lines are coupled. 500kW power was delivered per antenna, with a toroidal phasing $\Delta\phi=\pi/2$ rad. SOL density (n_e) distributions are measured by Lithium Beam Emission Spectroscopy (Li-BES) [8] and X-mode reflectometry [9], whose Lines Of Sight (LOS) have different magnetic connections to the various antennas (see Figure 1). D[H]-heated L-mode pulses at 2.4T were studied, where

*See the author list of “X. Litaudon et al. 2017 *Nucl. Fusion* **57** 102001”

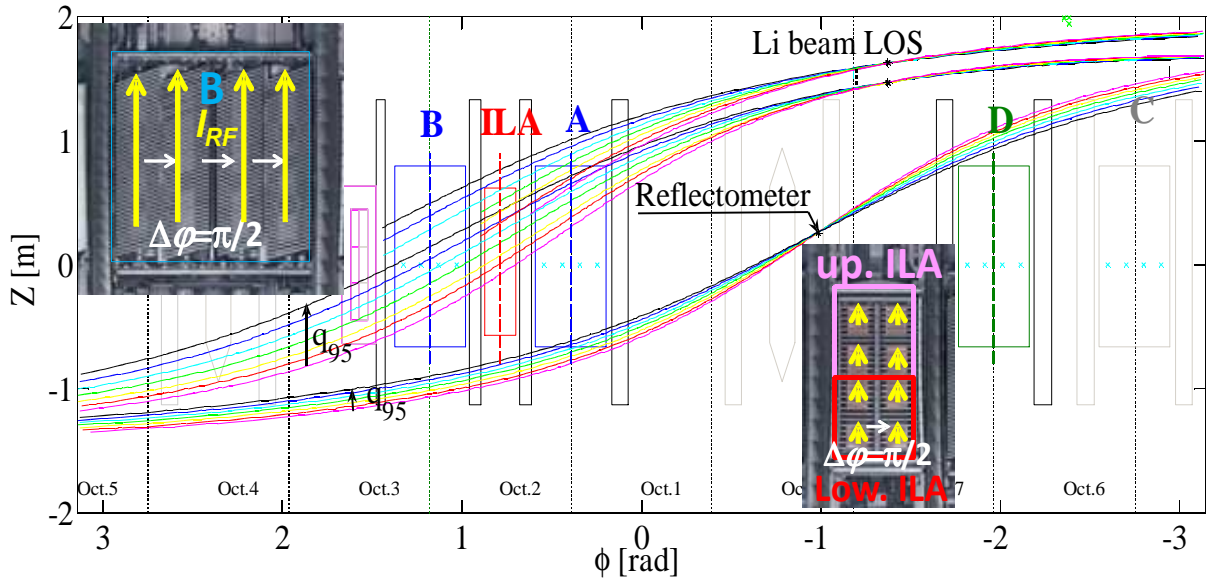


Figure 1: Toroidal/vertical view of ICRF antennas and outer limiters in JET from inside the vacuum vessel. Magnetic field line tracing from several points along Lithium beam and reflectometry LOS on pulse JPN 90454, over a scan of q_{95} . Inset: photos of A2 and ITER-like ICRF antennas, with sketch of the toroidal phasing.

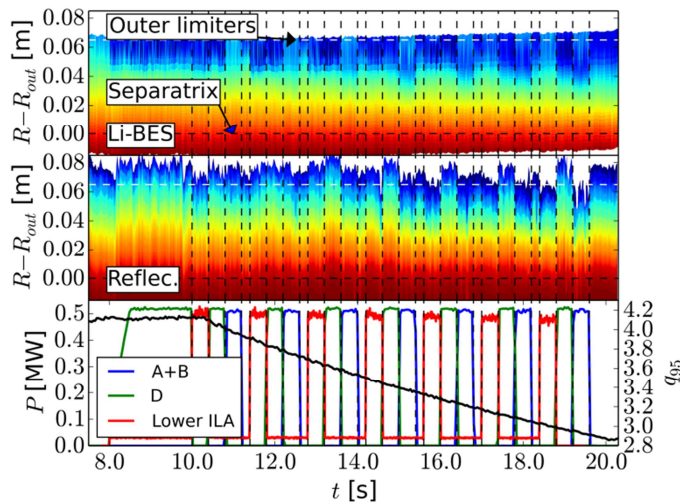


Figure 2: Time traces during pulse JPN 90456. Upper two panels: density distributions (logarithmic scale) along Li-beam and reflectometry LOS, mapped to outer mid-plane, *vs* time and radial distance to separatrix. n_e color range: $1 \times 10^{17} \text{ m}^{-3}$ to $1.2 \times 10^{19} \text{ m}^{-3}$. Bottom: RF power delivered by the different ICRF antennas, and edge safety factor q_{95} .

in magnitude with larger RF power and when switching from phasing $\Delta\phi = \pi$ to $\Delta\phi = \pi/2$ [4]. They depended on q_{95} , on which antenna was active and which diagnostic monitored n_e . This is attributed to varying LOS-antenna magnetic connections. Following this idea, supported by other observations (*e.g.* [5]), and assuming a parallel homogeneity of the RF-induced SOL patterns, the ratio of time-averaged n_e with or without RF waves was plotted *versus* the

ICRF antennas were toggled while the plasma current was ramped up (see figure 2). D_2 gas fueling from a toroidally-distributed valve was feedback-controlled to maintain a constant core density. In ohmic regime Li-BES and reflectometry measured similar profiles within a 4cm radial shift. During ICRH n_e modifications with respect to ohmic references at similar edge safety factor q_{95} , were recorded in the outer SOL, several meters away toroidally from the active antennas. Earlier studies showed that these reproducible changes increased

location of observation points along the diagnostic LOS, mapped in front of each RF antenna using field line tracing. In this technique, first proposed in [10], the LOS ensured the radial resolution of 2D maps, while scanning q_{95} provided their vertical resolution.

II. Experimental 2D maps of RF-induced density variations.

[Figure 3](#) maps density ratios during A2 antennas with respect to ohmic reference. Ratios in the range of 0.4 (depletion) to 2.5 (over-density) were observed, mostly in the outer SOL, extending radially 2-3cm in front of antenna limiters, with poloidal asymmetries.

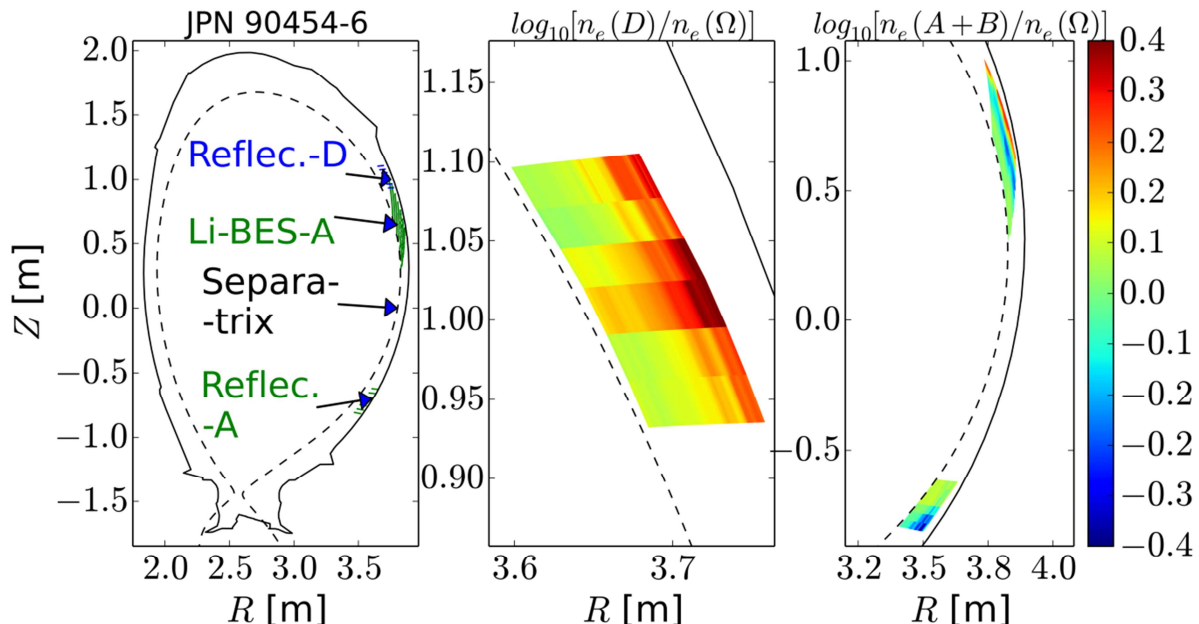


[Figure 3](#): 2D maps of n_e ratios during antenna D and A+B to ohmic, mapped to antennas D and A.

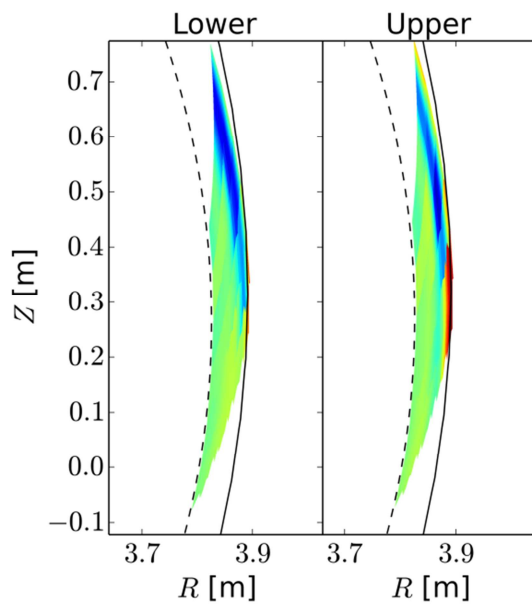


[Figure 4](#) compares n_e modifications when powering lower and upper ILA, along the Li-beam LOS connected magnetically to the upper array. n_e changes in this region even when the un-connected lower ILA is active. When switching to the upper array, the density depletion stays similar in the upper part of the map while an over-density area develops at the bottom.

[←Figure 4](#): $\log_{10}(n_e(\text{ILA})/n_e(\Omega))$ along Li-beam LOS mapped to ILA, with lower ILA (left panel, JPN 90456) and upper ILA (right panel, JPN 90509) active. Color scale: [-0.4 ;0.4].

III. Discussion and outlook.

Many machines have evidenced ICRF-induced SOL n_e modifications, with a phenomenology similar to JET [10-14]. The emitted oscillating near fields likely cause SOL biasing to large direct current (DC) potentials V_{DC} by RF-sheath rectification, and subsequent $\mathbf{E} \times \mathbf{B}$ n_e convection in $\mathbf{E}_{DC} = -\nabla_{\perp} V_{DC}$. Large V_{DC} exceeding sputtering thresholds [14-16] and SOL cross-field flows were measured during ICRH [14-17]. In addition to other experiments, *e.g.* [5], reproducing the observed n_e patterns, in relation with antenna electrical settings, can be used to validate RF-sheath modelling tools. Present simulations suggest that powering the

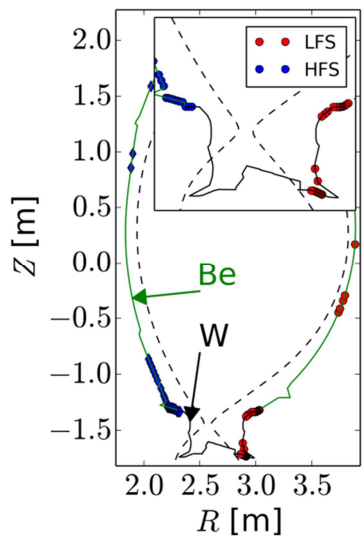


[Figure 5](#): (Radial-poloidal) location of connection points to the ILW for perturbed flux tubes along Li-beam LOS on pulse JPN 90454.

lower ILA with $\Delta\phi = \pi/2$ enhances V_{DC} also in the upper part of the antenna, but less than using the upper array, qualitatively consistent with [figure 4](#) [18]. Within RF-induced convection the maximal V_{DC} , most efficient for wall sputtering, is expected at the center of the convective cells. [Figure 5](#) shows that some flux tubes with modified n_e connect to W-components on the ILW, *e.g.* the tiles at low divertor entrance. Limited W spectroscopy diagnostics at these candidate sputtering locations and the toroidal spread of connection points, might explain why RF-specific W-sources have not yet been evidenced directly on the ILW [3]. This might guide further attempts at detection. It is also proposed to reduce RF-SOL interactions by tuning the power balance between inner and outer straps of A2 antennas [19].

Acknowledgements. This work has been carried out within the framework of the EUROfusion Consortium and has received funding from the European research and training programme under grant agreement N° 633053. The views and opinions expressed herein do not necessarily reflect those of the European Commission.

IV. References

- [1]: E. Lerche et al. *Nucl. Fus.* **56** (2016), 036022
- [2]: M. Goniche et al. *PPCF* **59** (2017) 055001
- [3]: V. Bobkov et al., *Journal of Nuclear Materials* **438** (2013) pp. S160–S165
- [4]: L. Colas et al. *JNM* **463** (2015) pp.735-738
- [5]: C.C. Klepper et al. *EPJ Web of Conferences* **157**, 03024 (2017)
- [6]: A. Kaye et al., SOFE Conf. Proc., 16th IEEE/NPSS Symposium, Vol. 1 p736 (1995)
- [7]: F. Durodié et al., *FED* **74**, 223–228 (2005)
- [8]: M. Brix, et al., *RSI* **81** (2010), 10D734
- [9]: A. Sironi, et al., *RSI* **81** (2010), 10D939
- [10]: L. Colas et al., *JNM* **363–365**, p.555 (2007)
- [11]: K. Cromb   et al. Proc. 40th EPS conference Espoo (Finland) 2013 ECA vol **37D** P4.184
- [12]: C. Lau et al. *PPCF* **55** (2013), 095003
- [13]: L. Colas et al., *AIP CP* **1580**, p.259 (2014)
- [14]: M.J. Martin et al. *PRL* **119** (2017) 205002
- [15]: R. Ochoukov et al. *PPCF* **56** (2014), 015004
- [16]: M. Kubi   et al. *Journal of Nuclear Materials* **438** (2013) S509–S512
- [17]: I. Cziegler et al. *PPCF* **54** (2012), 105019
- [18]: A. K  rvsk   et al., proc. 23rd PSI conf. Princeton 2018, P111, submitted to *Journ. Mat. & En.*
- [19]: Bobkov et al., proc. 23rd PSI conf. Princeton 2018, I106, submitted to *Journ. Materials & Energy*.